Syntheses of MnW12/TiO2 Microflowers and Nanorods for Photocatalytic H2 Evolution

Ningning Guo
Henan University
Shixian Liu
Henan University
Niuniu Zhang
Henan University
Xia Wu
Henan University
Guan Wang (wangguan@henu.edu.cn)
Henan University https://orcid.org/0000-0002-0082-1875
Yuan Zhao
Henan University

Nano Express

Keywords: isopolyoxometallate, controlling morphology, photocatalytic hydrogen generation

Posted Date: March 13th, 2021

DOI: https://doi.org/10.21203/rs.3.rs-304603/v1

Abstract

MnW_{12}/TiO_2 microflower has been successfully synthesized by the one-pot method and the microflower could be converted to nanorods by thermal treatment. The hydrogen evolution efficiency of MnW_{12}/TiO_2 nanorods is higher than that of MnW_{12}/TiO_2 microflowers by means of the photocatalysis test. These results suggest that the photocatalytic property of MnW_{12}/TiO_2 could be enhanced by controlling morphology. In addition, massive control experiments have been conducted to explore the effect factors of morphologies. Therefore, the successful preparations in this work not only open up new directions for the structural diversity of isopolyoxometallate based nano/micro materials, but also provide us with an irradiative way to increase the photocatalytic performance of POM/TiO_2 nano/micro composite.

1. Introduction

Polyoxometallates (POMs) as a fascinating species of metal–oxygen clusters have a wide range of potential applications due to their diverse structures and tunable properties in catalysis, materials and photoluminescence, etc [1-4]. As a unique branch of POM chemistry, POM based nano/micro materials remain less explored to date in comparison with traditional single crystal POM compounds. With the development of nanotechnology, the morphology, component and size of POM based nano/micro materials can be tuned easily through artificial methods. As a consequence, many researchers have been making significant efforts to explore in this field, and a variety of POM based nano/micro materials have been addressed [5-10]. In 2011, Cronin et al. reported a new phenomenon, namely, the growth of hollow mineral tubular architectures, and this may have significance in the interpretation of the architectures found in the fossil record that have been to date attributed to biological processes [7]. After this, Mn-based heteropolytungstate microspheres were prepared by Chattopadhyay and coworkers using a unique solvothermal method [11].

To the best of our knowledge, titanium dioxide (TiO_2) is an important photocatalyst and has been widely investigated due to its advantages such as relatively low-cost, good chemical stability and higher oxidation potential [12-17]. Zou's group fabricates TiO_2 p-n homojunction for photoelectrochemical and photocatalytic hydrogen generation [18]. Yi and coworkers reported W_2C@C/TiO_2 heterojunction architecture with efficient solar-light-driven hydrogen generation [19].

However, there are relatively few studies on the synthesis and properties of POMs/TiO_2 materials. In 2013, Bansal's group fabricated TiO_2-POM-bimetal nanocomposites for improved surface enhanced Raman scattering and solar light photocatalysis [20]. Wang et al. synthesized POM/TiO_2/Ag composite nanofibers with enhanced photocatalytic performance under visible light [21]. Lan's group reported POM/TiO_2 Fenton-like photocatalysts with rearranged oxygen vacancies for enhanced synergetic degradation [22]. From these literatures, the morphology is an important factor that has great impacts on the performance of photocatalyst. Because the morphology affects the specific surface area, separation efficiency and migration rate of photogenerated charges.

From these perspectives, how to enhance the performance of photocatalyst through morphology control has become a goal pursued by our group. In this work, MnW_{12}/TiO_2 microflower has been successfully prepared by a one-pot method through mild conditions. Fortunately, MnW_{12}/TiO_2 microflower could be converted to nanorods by thermal treatment at 550 °C. Under the photocatalysis test, the hydrogen evolution efficiency of MnW_{12}/TiO_2 nanorods is higher than that of MnW_{12}/TiO_2 microflowers. These results indicate that the performance of photocatalytic could be tuned by controlling morphology. Meanwhile, a large number of control experiments have been carried out to explore the effect factors of morphologies. Therefore, this work not only enrich the diversity of isopolyoxometallate based nano/micro materials, but also find an enlightening way to improve the photocatalytic efficiency of POM/TiO_2 nano/micro composite.

2. Experimental

2.1 Materials and methods

TiO_2 (P25) was purchased from Degussa. All chemicals were reagent-grade and used without further purification. The materials have been fully characterized by transmission electron microscope (TEM), scanning electron microscopy (SEM), energy dispersive X-ray spectroscopy (EDX), X-ray powder diffraction (XRD), IR spectroscopy, X-ray photoelectron spectroscopy (XPS), thermogravimetry (TG). XRD (Bruker D8 Advance, Bruker optics Instruments company, Karlsruhe, Germany) was performed using a instrument with Cu Kα radiation (λ = 1.5418 Å). The TEM images were obtained using a transmission electron microscope (JEM-2100F Electronics Co. LTD, Tokyo, Japan). The SEM images and EDX spectrum were obtained using a scanning electron microscope (JSM-7610F Electronics Co. LTD, Tokyo, Japan) with an acceleration voltage of 10 kV. The IR spectra were obtained via an Avatar 360 Fourier transform infrared spectrophotometer (Bruker optics Instruments company, Karlsruhe, Germany) using KBr pellets in the range of 4000–400 cm−1. XPS was conducted using a Thermo ESCALAB 250XI spectrometer (Thermo Fisher Scientific, Massachusetts, USA). The TG curve was obtained on the STA449F5 thermo-gravimetric analyzer (Netzsch, Selb, Germany).

2.2 Synthesis of MnW_{12} Microflower

$Na_2WO_4{\cdot}2H_2O$ (3.00 g, 9.62 mmol) was dissolved in 30 mL of distilled water, heated to 80 °C with stirring, and boric acid (0.10 g, 1.62 mmol) was added to the solution. Then, after adjusting the pH of the solution to 7.0 with dilute HCl, a small amount of aqueous solution containing $MnCl_2{\cdot}4H_2O$ (0.40 g, 2.00 mmol) was slowly added dropwise, and after the dropping, it was heated and stirred for the first 30 minutes. Then, after adjusting the pH of the solution to 6.0 with dilute HCl, it was heated and stirred for the second 30 minutes, finally cooled at room temperature for 1 hr. The MnW_{12} microflowers were collected by centrifugation and washed with water and ethanol to remove excess reagents. MnW_{12} microflowers

changed into different morphologies after calcination at different temperatures and atmospheres for 2 hrs.

2.3 Related Control Experiments

To explore the influence of different counter cations on the morphology, the synthetic procedure was identical to that of MnW_{12} microflowers, but $MnCl_2{\cdot}4H_2O$ was replaced by NH_4Cl, KCl, $N(C_4H_9)_4Br$, CsCl, respectively.

To explore the influence of different manganese salts on the morphology of MnW_{12} microflowers, the synthetic procedure was identical to that of MnW_{12} microflowers, but $MnCl_2{\cdot}4H_2O$ was replaced by $Mn(Ac)_2$, $Mn(ClO_4)_2$, $MnSO_4$, $Mn(NO_3)_2$, respectively.

To explore the influence of adding different amounts of PEG4000 on the MnW_{12} microflowers, the synthetic procedure was identical to that of MnW_{12} microflowers, but different amounts of PEG4000 were added to the solution after boric acid.

To explore the influence of different stirring times on the appearance of MnW_{12} microflowers, the synthetic procedure was identical to that of MnW_{12} microflowers, but the first 30 minutes were changed to 10 min, 1 hr, 2 hrs, respectively.

To explore the influence of different amount of $MnCl_2$ on the appearance of MnW_{12} microflowers, the synthetic procedure was identical to that of MnW_{12} microflowers, but the amount of $MnCl_2$ were changed to 1 mmol, 4 mmol, respectively.

2.4 Synthesis of MnW_{12}/TiO_2 Microflowers

$Na_2WO_4{\cdot}2H_2O$ (3.00 g, 9.62 mmol) was dissolved in 30 mL of distilled water, heated to 80 °C with stirring, and boric acid (0.10 g, 1.62 mmol) was added to the solution. Then, after a small amount of aqueous solution containing TiO_2 (0.12g, 1.50mmol) was slowly added dropwise, adjusting the pH of the solution to 7.0 with dilute HCl, a small amount of aqueous solution containing $MnCl_2{\cdot}4H_2O$ (0.40 g, 2.00 mmol) was slowly added dropwise, and after the dropping, it was heated and stirred for the first 30 minutes. Then, after adjusting the pH of the solution to 6.0 with dilute HCl, it was heated and stirred for the second 30 minutes, and finally cooled at room temperature for 1 hr. MnW_{12}/TiO_2 microflowers were collected by centrifugation and washed with water and ethanol to remove excess reagents.

2.5 Synthesis of MnW_{12}/TiO_2 Nanorods

The MnW_{12}/TiO_2 microflowers (3 g) was placed in a porcelain boat and transferred to a tube furnace at room temperature. Then the temperature was ramped to 550 °C at a speed of 5 °C min^{-1} and maintained for 2 h under air atmosphere. After cooling to room temperature, MnW_{12}/TiO_2 nanorods were collected.

2.6 Photocatalytic Hydrogen Production

The H_2 evolution experiments were performed in a closed gas-circulating system CEL-PAEM-D8 (China Education Au-light Co., Ltd, Beijing, China) equipped with an external illumination Pyrex reaction vessel (total volume 100 mL) with a magnetic stirrer for vigorous stirring and analyzed by using an automatic H_2 monitoring system. The vessel was filled with a solution containing a sacrificial electron donor CH_3OH (25 mL), H_2O (25 mL), H_2PtCl_6 (0.012 g) and different catalysts. The reaction was tested using a 300 W Xe light (350–780 nm) and the system was evacuated (–0.1MPa) before opening the Xe light. The produced H_2 was analyzed by a gas chromatography (GC7900) with a TCD using Ar as the carrier gas.

3. Results And Discussion

In the past two decades, many researchers have been working on the morphology and composition of POM based nano/micro materials. However, the progress shows slower in comparison with traditional single-crystal compounds. In addition, morphologies of POM based nano/micro materials are not abundant, compared with other nano/micro materials. Only few morphologies have been characterized, such as polyhedron, tube, wire and spheres. As shown in Scheme 1, the materials based on isopolyoxometallate are rarely reported in recent years. As a unique branch of POM compound, isopolyoxometallate materials lack of sufficient concern. Finally, the controllable synthesis and photocatalytic hydrogen production properties of POM/TiO_2 nano/micro composite are rarely studied until now. Therefore, we are making great efforts to explore the design and syntheses of isopolyoxometallate based material and research the photocatalytic hydrogen production. Then the combination of MnW_{12} and TiO_2 would create new functional material.

3.1 SEM and TEM images

First of all, Scheme S1 shows a schematic of the synthetic processes used to prepare the MnW_{12} microflower. During the procedure, Mn^{2+} plays the role as counter ions which would be combined with polyanions. As shown in Figure 1, the MnW_{12} microflower is composed of uniform flower-like morphology. After statistic of 60 particles, the diameter is distributed in the range of 1.5–1.8 μm and the average diameter is around 1.55 μm (Figure 1a, inset). Figure 1c–d show the typical transmission electron microscope (TEM) and the high resolution TEM (HRTEM) images of MnW_{12} microflower. The flower-like morphology of MnW_{12} is also verified by TEM and the d-spacing (0.3 nm) of the MnW_{12} microflower is observed by HRTEM. The novel flower-like morphology based on W_{12} was currently rarely reported, and this result was far beyond our expectation. Thus, great efforts were also put into studying

the different variables in the formation of the materials. Scheme S2 shows the summary of morphology changes based on $[H_2W_{12}O_{40}]^{6-}$ (referred as 'W_{12}' for short) in this work. This shows POM based nano/micro materials based on W_{12} have great potential in morphology and performance, and are worthy of exploration and research.

In the process of synthesizing MnW_{12}, TiO_2 is doped to obtain MnW_{12}/TiO_2 microflowers (Figure 2a), which are calcined to obtain MnW_{12}/TiO_2 nanorods (Figure 2b). As shown in Figure 2a, although the morphology of MnW_{12} is slightly changed due to the addition of TiO_2, MnW_{12}/TiO_2 still maintains the morphology of microflowers. To our astonishment, MnW_{12}/TiO_2 microflowers can be transformed to MnW_{12}/TiO_2 nanorods by thermal treatment at 550 °C for 2 hrs. The two different morphologies of MnW_{12}/TiO_2 are rare in POM/TiO_2 nano/micro composite materials, which also lay the foundation for the different photocatalytic properties. Figure 2c–d show the typical transmission electron microscope (TEM) and the high resolution TEM (HRTEM) images of MnW_{12}/TiO_2 microflowers and MnW_{12}/TiO_2 nanorods. As shown in Figure 2c and Figure 2d (inset, left), the d-spacing (0.24 nm) of the MnW_{12}/TiO_2 microflowers and the d-spacing (0.3 nm) of the MnW_{12}/TiO_2 nanorods are observed by HRTEM, which is according to that of MnW_{12} microflower. As depicted in Figure 2c and Figure 2d (inset, right), the other d-spacing (0.35 nm) of the MnW_{12}/TiO_2 microflowers and the other d-spacing (0.39 nm) of the MnW_{12}/TiO_2 nanorods can be readily indexed to the {101} d-spacing (0.35 nm) of the anatase TiO_2. From the above discussion, it can be concluded that MnW_{12}/TiO_2 microflowers and nanorods are composed of MnW_{12} and TiO_2. In order to further identify the components of the MnW_{12}/TiO_2 microflowers and nanorods, the corresponding EDX spectrum and element mapping were investigated (Figure S8 and Figure S9). The analyses evidently prove the presence of Mn, W, Ti, Na and O components. Furthermore, the element mapping of Mn, W, Ti, and Na shows a homogeneous distribution in the MnW_{12}/TiO_2 microflowers and nanorods.

3.2 IR spectra

Meanwhile, the IR spectra of MnW_{12}/TiO_2 microflowers, MnW_{12} and MnW_{12}/TiO_2 nanorods, MnW_{12}-Air-550 °C were obtained between 400 and 4000 cm^{-1} using KBr pellets, which is very useful for the identification of the characteristic vibration bands of the POMs in the products. As depicted in Figure 3a, MnW_{12}/TiO_2 microflowers could be identified by three characteristic IR bands appearing at 864 cm^{-1} (v WO_t), 812 cm^{-1} (v W_2O, corner) and 661 cm^{-1} (v W_2O, edge), which is in accordance with the bulk $[H_2W_{12}O_{40}]^{6-}$. And the bands at 913 cm^{-1}, 876 cm^{-1}, 812 cm^{-1} and 653 cm^{-1} for MnW_{12} are attributed to the vibration of the above v(W-O) bonds. As shown in Figure 3b, The bands at 872, 830, and 702 cm^{-1} are observed for MnW_{12}/TiO_2 nanorods, which are attributed to the (v WO_t), (v W_2O, corner), and (v W_2O, edge) bonds, respectively. In addition, the occurrence of the characteristic vibration at 878, 799 and 727 cm^{-1} confirms the v(W-O) bonds of MnW_{12}-Air-550 °C. These results indicate the building blocks of

MnW_{12}/TiO_2 microflowers, MnW_{12} and MnW_{12}/TiO_2 nanorods, MnW_{12}-Air-550 ℃ are all based on isopolyoxometallates $[H_2W_{12}O_{40}]^{6-}$ and the polyanions are preserved after calcining.

3.3 XRD patterns

The as-prepared MnW_{12}/TiO_2 microflowers, MnW_{12}/TiO_2 nanorods and their precursors were characterized by XRD. As can be seen from Figure 4a, the main peaks of MnW_{12}/TiO_2 microflowers at 25.34°, 36.06°, 38.51°, 47.98°, 53.94°, 55.05°, 62.72° and 68.94° can be readily indexed to the anatase TiO_2. According to the standard cards of anatase TiO_2 (pdf no. 894921), the above-mentioned 2θ peaks are attributed to (101), (103), (112), (200), (105), (211), (204) and (116) crystal planes, respectively. And the peak of MnW_{12}/TiO_2 microflowers at 27.41° is assigned to the (110) crystal plane of the rutile TiO_2. The results reveal that the P25-TiO_2 is preserved in the final product. Besides, the main 2θ peaks of MnW_{12}/TiO_2 microflowers at around 18.27°, 23.67°, 34.91°, 37.42°, 41.03°, 52.03° and 62.17° can be readily indexed to the MnW_{12}, which manifests MnW_{12} is the building block of the MnW_{12}/TiO_2 microflowers. As shown in Figure 4b, The main 2θ peaks of MnW_{12}/TiO_2 nanorods at around 25.35°, 48.23°, 54.72° and 63.09° are assigned to the (101), (200), (105) and (204) crystal planes of anatase TiO_2, respectively. In addition, the main peaks of MnW_{12}/TiO_2 nanorods at 18.37°, 23.54°, 29.87°, 35.98°, 40.96°, 44.17°, 49.25°, 51.25° and 64.6° can be readily indexed to the MnW_{12}-Air-550 ℃. These results show that the composition of MnW_{12}/TiO_2 nanorods is definite, which consist of TiO_2-Air-550 ℃ and MnW_{12}-Air-550 ℃.

3.4 XPS spectra

In addition, the XPS investigations on MnW_{12}/TiO_2 microflowers and MnW_{12}/TiO_2 nanorods were recorded to confirm the valence states of Mn, W and Ti. As the valence states of Mn, W and Ti of MnW_{12}/TiO_2 microflowers and MnW_{12}/TiO_2 nanorods are the same (Figure S10), take MnW_{12}/TiO_2 nanorods as the example for detailed description. As depicted in Figure S10d, the peaks around 639.7 and 652.5 eV in the energy regions of Mn_{2p} correspond to Mn^{2+} ions, indicating the existence of transition metal ion in this nanocomposites. As shown in Figure S10e, the peaks around 34.4 and 36.5 eV in the energy regions of W_{4f} are confirmed to the W^{6+} centers in $[H_2W_{12}O_{40}]^{6-}$ building blocks. And the Ti_{2p} XPS peaks have a binding energy of 458.4 eV and 464.4 eV, respectively, indicating that Ti^{4+} ion is incorporated into the nanorods (Figure S10f).

3.5 TG analysis

The Netzsch STA449F5 thermo-gravimetric analyzer was used for the thermal analysis in nitrogen dynamic atmosphere (50 mL/min) at a heating rate of 10 K/min and 19.2285 mg powder of MnW_{12}/TiO_2 microflowers was thermally treated (Figure 5). The TG curve gives a total weight loss of 6.41% in the range of 23-1000 ℃. The weight loss of 2.68% during the first step from 23 to 164 ℃ corresponds to the

release of adsorbed water molecules. On further heating, the second weight loss of 3.73% between 164-290 ℃ is approximately attributed to the removal of structural water molecules.

3.6 Photocatalytic hydrogen generation

As depicted in Figure 6a, the hydrogen production of MnW_{12}/TiO_2 microflowers is 21.966 mmol g-1, and the hydrogen production of MnW_{12}/TiO_2 nanorods is 28.684 mmol g-1, after 5 hrs of light irradiation. And it is calculated that the hydrogen production of MnW_{12}/TiO_2 nanorods is 30.58% higher than that of MnW_{12}/TiO_2 microflowers. The higher photocatalytic activity for MnW_{12}/TiO_2 nanorods than MnW_{12}/TiO_2 microflowers is probably due to the differences in morphologies of MnW_{12}/TiO_2, which will be explained from the following two aspects. On the one hand, the different morphologies of MnW_{12}/TiO_2 endow them different specific surface areas. As shown in Figure 6c, d and Table 1, the specific surface area of MnW_{12}/TiO_2 nanorods is higher than that of MnW_{12}/TiO_2 microflowers. A larger specific surface area can provide more active sites, which contributes to the release of more hydrogen in the photocatalytic process. On the other hand, the morphology affects the separation efficiency and migration rate of photogenerated charges. Due to the quantum size effect, the particle size becomes smaller from microflowers to nanorods. In this case, charges separation effect and migration efficiency become higher, which leads to the improvement of catalytic activity. In short, the morphologies of MnW_{12}/TiO_2 are not alike, resulting in different photocatalytic hydrogen production capabilities. In addition, the stability test of MnW_{12}/TiO_2 nanorods showed that the total hydrogen production of three cycles were 28.051 mmol/g, 25.381 mmol/g and 25.332 mmol/g, respectively (Figure 6b). After long-term illumination of 15 hours, the MnW_{12}/TiO_2 nanorods still maintain the corresponding catalytic activity. Meanwhile, there is no significant change in the XRD pattern of MnW_{12}/TiO_2 nanorods before and after three cycles of photocatalytic hydrogen generation (Figure S11). In all, the above confirm that MnW_{12}/TiO_2 nanorods have relatively favorable photocatalytic activity and cycle stability.

4. Conclusion

In summary, MnW_{12}/TiO_2 microflowers were successfully prepared by one-pot method under mild conditions. Moreover, the microflowers turn into nanorods though thermal treatment. The hydrogen production efficiency of MnW_{12}/TiO_2 nanorods is better than that of MnW_{12}/TiO_2 microflowers through the photocatalytic hydrogen production test. The difference in photocatalytic performance is attributed to the difference in morphology. Meanwhile, a large number of control experiments have also been explored to clarify the reasons for the transformation of morphology. Thus, the successful preparation of MnW_{12}/TiO_2 microflowers and nanorods enrichs the structural diversity of isopolyoxometallate based nano/micro materials. And this method reported in this work is proposed to be a general process to improve the photocatalytic efficiency of POM/TiO_2 nano/micro composite.

Declarations

Authors'Contributions

Conceptualization—investigation: N.G., G.W. and Y.Z.; writing—review and editing: N.G. and G.W.; validation: S.L., N.Z., X.W.; funding acquisition: G.W.. All authors have approved the final version of the manuscript.

Funding

This work was supported by the Natural Science Foundation of China (Grants: 21901061 and U1504201). The authors are grateful to the Program for Science & Technology Innovation Talents in Universities of Henan Province (19HASTIT004) and the Program for Innovation Teams in Science and Technology in Universities of Henan Province (20IRTSTHN004).

Availability of Data and Materials

Data sharing is not applicable to this article as no datasets were generated or analyzed during the current study.

Competing interests

The authors declare that they have no conflict of interests.

References

[1] Yamase, T. (1998). Photo- and electrochromism of polyoxometalates and related materials. Chem. Rev. 98: 307–325.

[2] Long, D.L.; Burkholder, E.; Cronin, L. (2007). Polyoxometalate clusters, nanostructures and materials: from self-assembly to designer materials and devices. Chem. Soc. Rev. 36: 105–121.

[3] Mizuno, N.; Yamaguchi, K.; Kamata, K. (2005). Epoxidation of olefins with hydrogen peroxide catalyzed by polyoxometalates. Coord. Chem. Rev. 249: 1944–1956.

[4] Song, Y.F.; Tsunashima, R. (2012). Recent advances on polyoxometalate-based molecular and composite materials. Chem. Soc. Rev. 41: 7384–7402.

[5] Liu, T.B.; Diemann, E.; Li, H.L.; Dress, A.W.M.; Müller, A. (2003). Self-assembly in aqueous solution of wheel-shaped Mo_{154} oxide clusters into vesicles. Nature, 426: 59–62.

[6] Zhang, L.J.; Webster, T.J. (2009). Nanotechnology and nanomaterials: promises for improved tissue regeneration. Nanotoday 4: 66–80.

[7] Cooper, G.J.T.; Boulay, A.G.; Kitson, P.J.; Ritchie, C.; Richamond, C.J.; Thiel, J.; Gabb, D.; Eadie, R.; Long, D.L.; Cornin, L. (2011). Osmotically driven crystal morphogenesis: a general approach to the fabrication of

micrometer-scale tubular architectures based on polyoxometalates. J. Am. Chem. Soc. 133: 5947–5954.

[8] Shen, Y.; Peng, J.; Zhang, H.Q.; Yu, X. (2012). Mo-substituted Keggin tungstosilicate microtubes: preparation and characterization. Inorg. Chem. 51: 5146–5151.

[9] Wang, G.; Meng, R.R.; Yang, J.; He, X.M.; Chen, J.J.; Zhang, D.D.; Xu, X.X.; Niu, J.Y. (2019). Shape-control of CeF_3 nanocrystals by doping polyoxometalates: syntheses, characterization and tunable photoluminescence. Chem. Commun. 55: 1619–1622.

[10] Wang, G.; Wang, Y.K.; Meng, R.R.; Xu, X.X.; Niu, J.Y. (2018). Synthesis and spectroscopic properties of silver-fluorescein co-doped phosphotungstate hollow spheres. Dalton. Trans. 47: 7730–7738.

[11] Bhattacharjee, K.; Chattopadhyay, K.K.; Das, G.C. (2015). Unconventional dexter-silverton type manganese heteropolytungstate [$Mn_7(MnW_{12}O_{42}(OH)_4{\cdot}8H_2O)$] hollow microsphere: synthesis, crystal structure, growth mechanism, and optical property study. J. Phys. Chem. C. 119: 1536-1547.

[12] Schattka, J.H.; Shchukin, D.G.; Jia, J.G.; Antonietti, M.; Caruso, R.A. (2002). Photocatalytic activities of porous titania and titania/zirconia structures formed by using a polymer gel templating technique. Chem. Mater. 14: 5103-5108.

[13] Luo, H.M.; Takata, T.; Lee, Y.; Zhao, J.F.; Domen, K.; Yan, Y.S. (2004). Photocatalytic activity enhancing for titanium dioxide by co-doping with bromine and chlorine. Chem. Mater. 16: 846-849.

[14] Parayil, S.K.; Lee, Y.M.; Yoon, M. (2009). Photoelectrochemical solar cell properties of heteropolytungstic acid-incorporated TiO_2 nanodisc thin films. Electrochemistry Communications 11: 1211–1216.

[15] Xu, Y.F.; Zhang, C.; Zhang, L.X.; Zhang, X.H.; Yao, H.L.; Shi, J.L. (2016). Pd-catalyzed instant hydrogenation of TiO_2 with enhanced photocatalytic performance. Energy Environ. Sci. 9: 2410-2417.

[16] AlSalka, Y.; Hakki, A.; Schneider, J.; Bahnemann, D.W. (2018). Co-catalyst-free photocatalytic hydrogen evolution on TiO_2: synthesis of optimized photocatalyst through statistical material science. Appl. Catal. B Environ. 238: 422-433.

[17] Hu, L.S.; Li, Y.; Zheng, W.R.; Peng, Y.K.; Tsang, S.C.E.; Lee, L.Y.S.; Wong, K.Y. (2020). Blue ordered/disordered Janus-type TiO_2 nanoparticles for enhanced photocatalytic hydrogen generation. J. Mater. Chem. A 8: 22828-22839.

[18] Pan, L.; Wang, S.B.; Xie, J.W.; Wang, L.; Zhang, X.W.; Zou, J.J. (2016). Constructing TiO_2 p-n homojunction for photoelectrochemical and photocatalytic hydrogen generation. Nano Energy 28: 296-303.

[19] Yue, X.Z.; Li, C.Q.; Liu, Z.Y.; Yi, S.S.; Chen, D.L.; Wang, F.; Li, S.H. (2019). Steering charge kinetics in W_2C@C/TiO_2 heterojunction architecture: efficient solar-light-driven hydrogen generation. Appl. Catal. B Environ. 255: 117760-117769.

[20] Pearson, A.; Bhosale, S.; Bhargava, S.K.; Bansal, V. (2013). Combining the UV-switchability of Keggin ions with a galvanic replacement process to fabricate TiO_2-polyoxometalate-bimetal nanocomposites for improved surface enhanced raman scattering and solar light photocatalysis. ACS Appl Mater Interfaces 5: 7007-7013.

[21] Shi, H.F.; Yu, Y.C.; Zhang, Y.; Feng, X.J.; Zhao, X.Y.; Tan, H.Q.; Khan, S.U.; Li, Y.G.; Wang, E.B. (2018). Polyoxometalate/TiO_2/Ag composite nanofibers with enhanced photocatalytic performance under visible light. Appl. Catal. B Environ. 221: 280-289.

[22] An, X.Q.; Tang, Q.W.; Lan, H.C.; Liu, H.J.; Qu, J.H. (2019). Polyoxometalates/TiO_2 Fenton-like photocatalysts with rearranged oxygen vacancies for enhanced synergetic degradation. Appl. Catal. B Environ. 244: 407-413.

Tables

Table 1. The specific surface area and pore size of MnW_{12}/TiO_2 microflowers and MnW_{12}/TiO_2 nanorods.

Sample	Specific surface area (m^2/g)	pore size (nm)
MnW_{12}/TiO_2 microflowers	24.592	3.820
MnW_{12}/TiO_2 nanorods	29.302	3.817

Figures

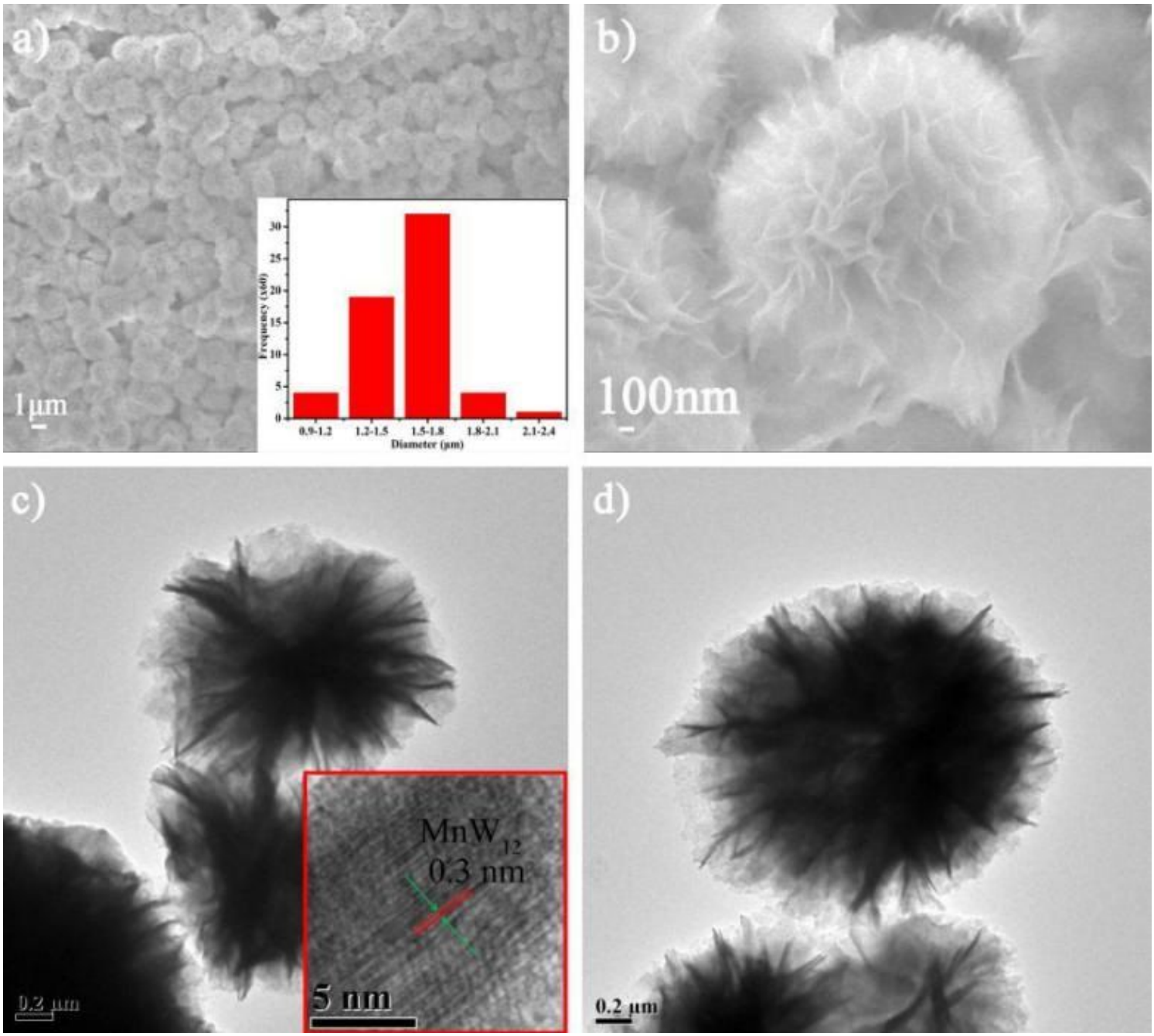

Figure 1

(a and b) SEM images of MnW12 microflower with different resolutions, inset: size distribution of MnW12 microflower; (c and d) TEM/HRTEM images of MnW12 microflower.

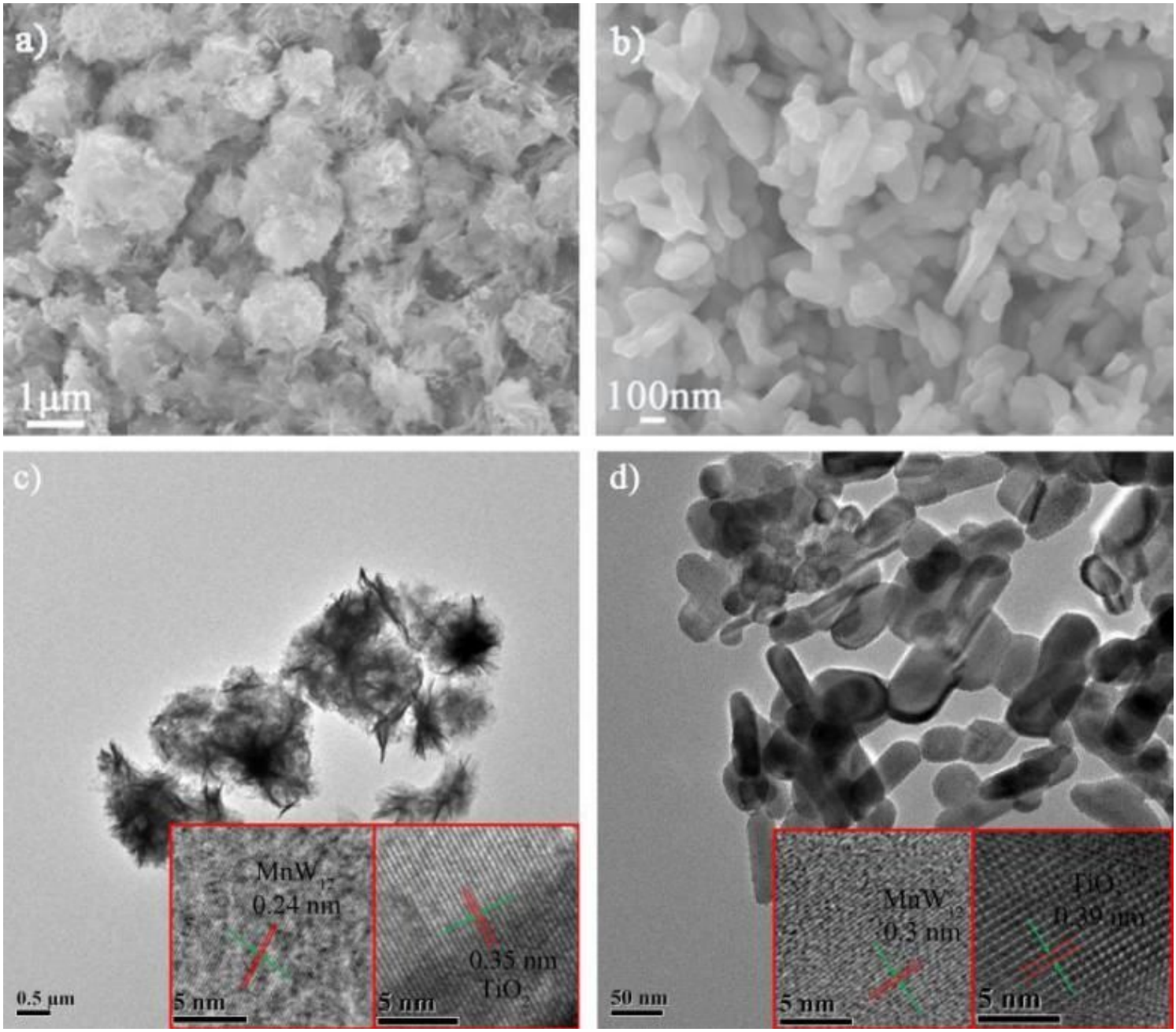

Figure 2

(a and b): SEM images of MnW12/TiO2 microflowers (a) and MnW12/TiO2 nanorods (b); (c and d): TEM/HRTEM images of MnW12/TiO2 microflowers (c) and MnW12/TiO2 nanorods (d).

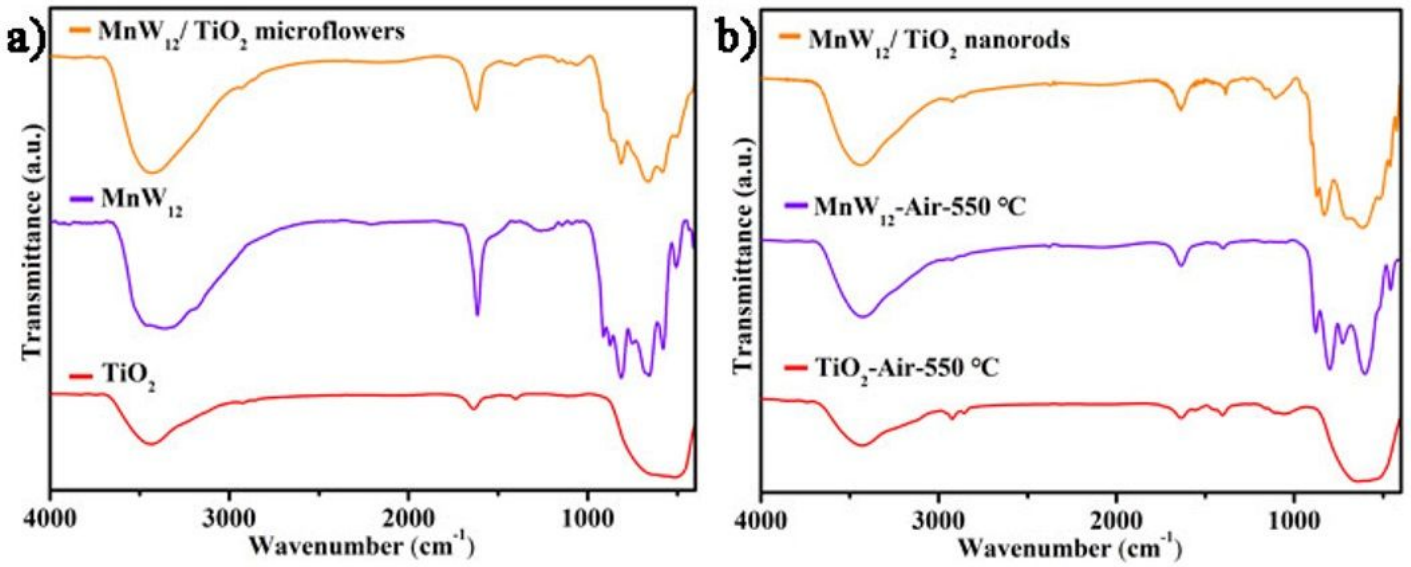

Figure 3

(a): The IR spectra of MnW12/TiO2 microflowers, MnW12 and TiO2; (b): the IR spectra of MnW12/TiO2 nanorods, MnW12-Air-550 °C and TiO2-Air-550 °C.

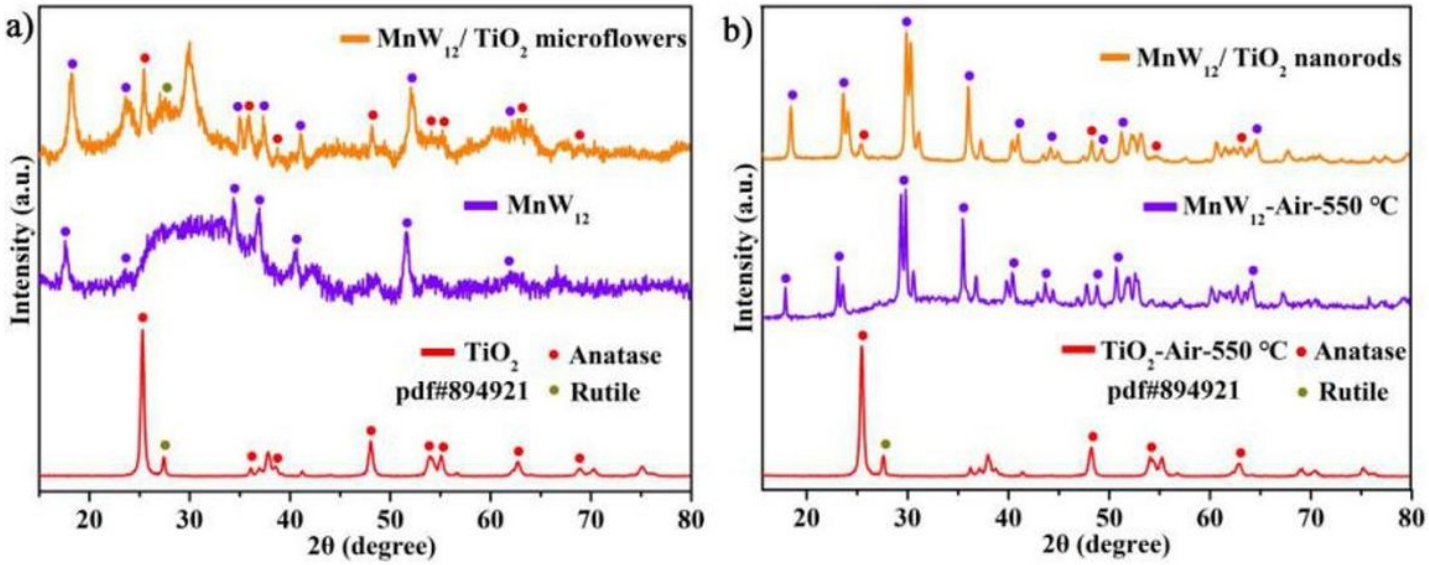

Figure 4

(a): The XRD pattern of MnW12/TiO2 microflowers, MnW12 and TiO2; (b): the XRD pattern of MnW12/TiO2 nanorods, MnW12-Air-550 °C and TiO2-Air-550 °C.

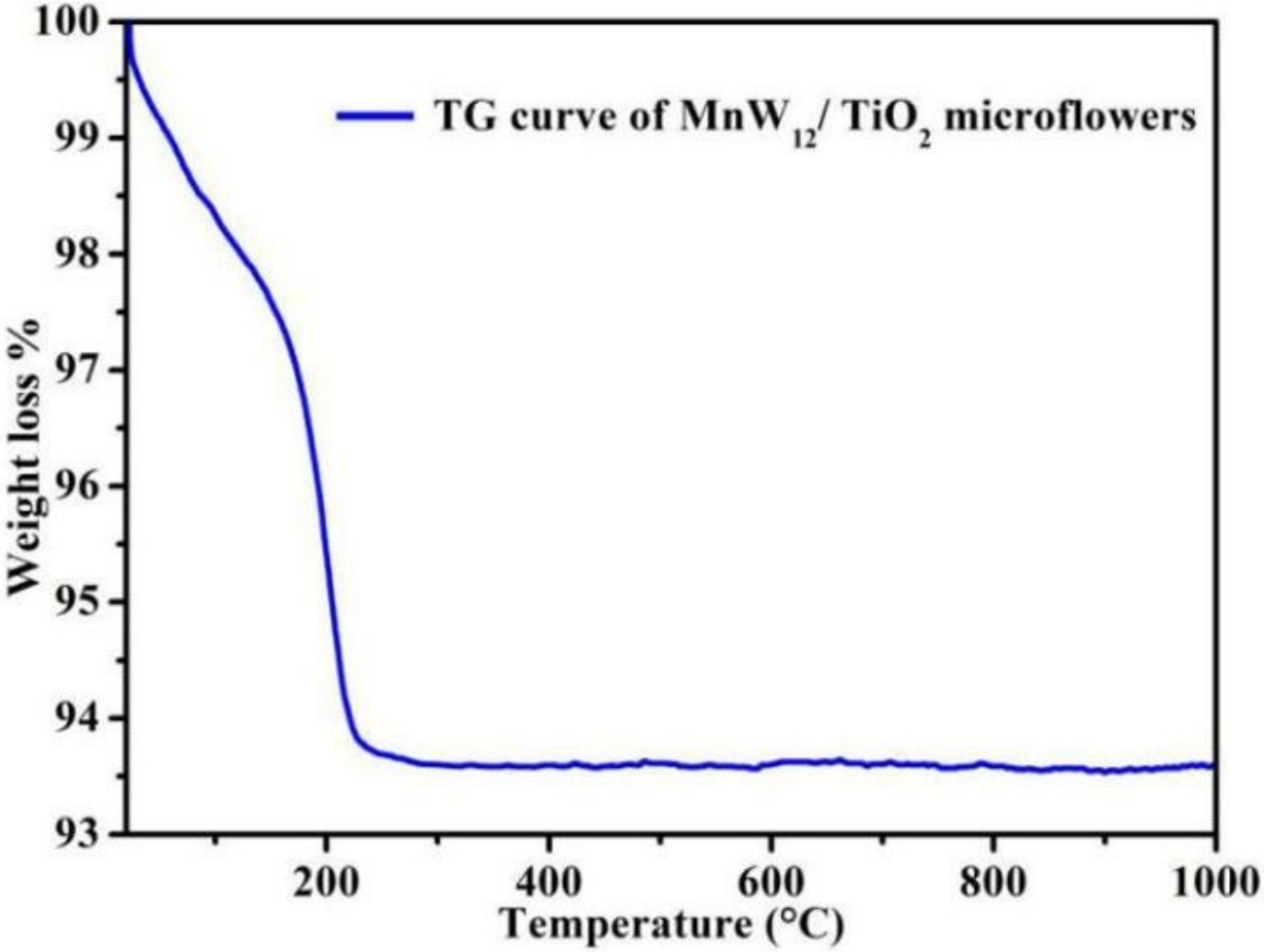

Figure 5

The TG spectra of MnW12/TiO2 microflowers.

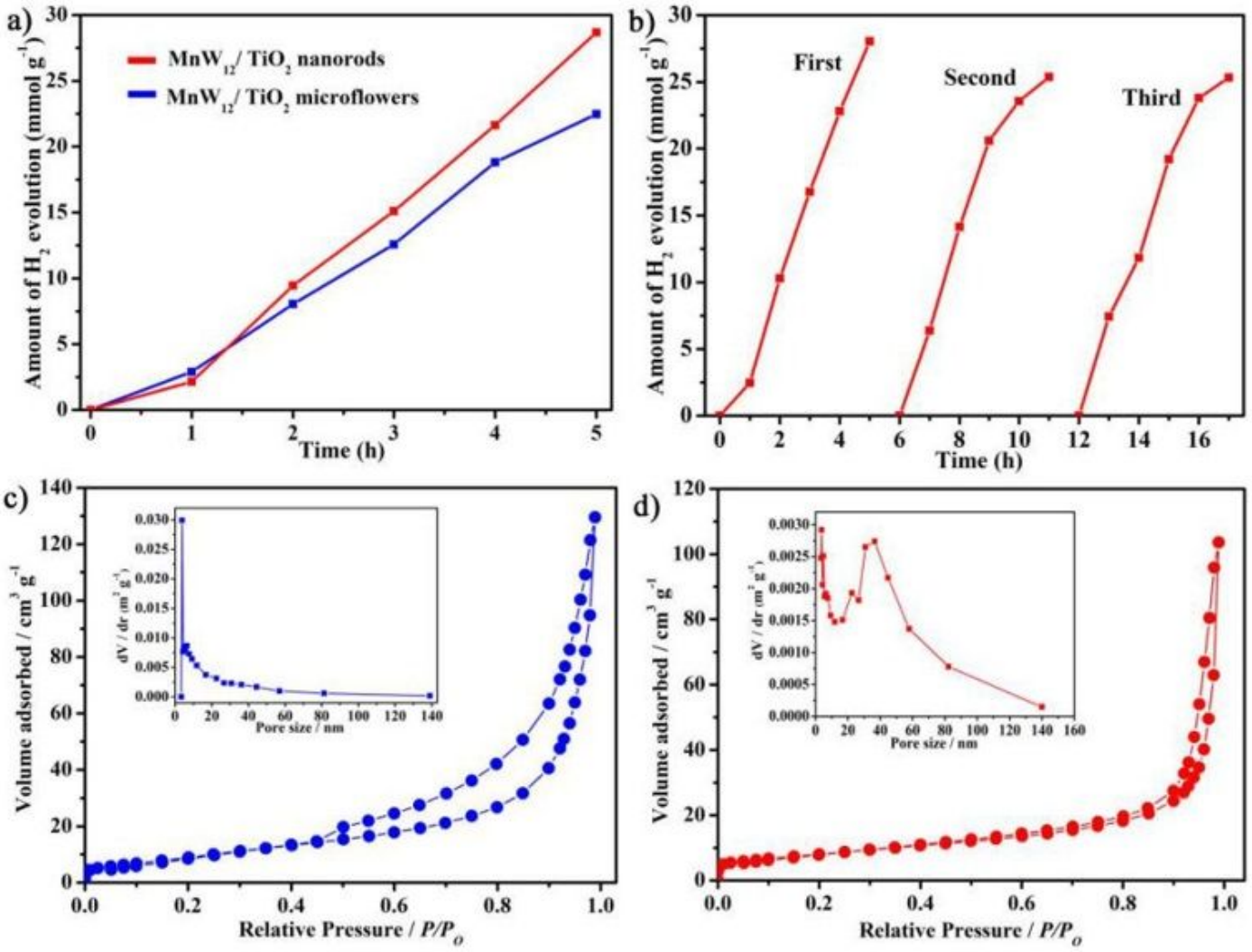

Figure 6

(a): Time course of photocatalytic hydrogen generation between MnW12/TiO2 microflowers and MnW12/TiO2 nanorods; (b): Photocatalytic hydrogen generation of MnW12/TiO2 nanorods with intermittent evacuation every 5 h; (c and d): N2 adsorption-desorption isotherm of MnW12/TiO2 microflowers (c) and MnW12/TiO2 nanorods (d), (inset: the corresponding pore size distribution curve).

Supplementary Files

This is a list of supplementary files associated with this preprint. Click to download.

- Scheme1.jpeg
- SupportingInformation.docx